Journal of Applied Sciences

ISSN 1812-5654

science alert

ANSInet
an open access publisher
http://ansinet.com

Journal of Applied Sciences 13 (22): 5298-5308, 2013
ISSN 1812-5654 / DOI: 10.3923/jas.2013.5298.5308

Analysis of Guided Waves in Adhesively Bonded Composite Structures

Zhang Hong
School of Science, Chang'an University, Xi'an, 710064, China

Abstract: Characteristics of guided wave in adhesively bonded composite structures are studied in this paper. Hamilton's principle and semi-analytical finite element method are combined to formulate equations of motion and dispersion. Material property in the composite is expressed in the global coordinate system through rotation matrix. In numerical calculation, a 16 layer adhesively bonded composites is investigated. Results showed that phase velocity dispersion curves decreased slightly when states of adhesive layer changing from properly bonded to disbond in plate model and variation in pipe model is noticeable.

Key words: Guided wave, adhesively bonded, composite structures, semi-analytical finite element method

INTRODUCTION

Adhesively bonded composite structures have been used widely in aerospace and automotive industries as a direct alternative to riveting. It offers several benefits for the joining of materials: (1) The ability to uniformly distribute loads across the entire joint area, (2) The ability to join thin or thick materials of any shape, (3) The ability to attenuate mechanical vibrations and sound, (4) The ability to minimize or prevent galvanic corrosion between dissimilar materials due to their low electrical conductivity, (5) Excellent ability to resist fatigue and cyclic loads, (6) Much faster and more cost-effective than mechanical method. But the quality assessment of adhesively bonded components still remains a long-standing challenge in the field of nondestructive technology NDT. Guided waves inspection of adhesively bonded structures has gone through decades of improvement and has proven to be a very powerful method.

Matt *et al*. (2005) and Matt (2007) presented the monitoring of adhesively bonded joints by ultrasonic guided waves and examined the wing skin-to-spar bonds of unmanned aerial vehicles, the assessment of bond state is based on monitoring the strength of transmission through the joints of selected guided modes. Di Scalea *et al*. (2004) studied the propagation of ultrasonic guided waves in adhesively bonded lap-shear joints by using the lowest-order, antisymmetric mode. Lowe *et al*. (2000) investigated the transmission of Lamb waves across adhesively bonded lap joints using finite element method by considering three modes for excitation and reception, which provided a basis for the selection of modes for NDE of the bond region. Allin *et al*. (2003) described a robust technique for the detection of disbands, based on the fundamental through-thickness resonance frequency of a joint of automotive components. Higgins (2000) presented details and history of the main adhesives used in the construction of British Aerospace and predecessors commercial aircraft with some details of adhesive bonding used by other aircraft manufacturers. Brotherhood *et al*. (2003) studied the detectability of dry contact kissing bonds in adhesive joints using three ultrasonic inspection techniques. Duflo *et al*. (2007) studied the characterization of defects in the bonding of two carbon epoxy composite plates using Lamb waves. Seifried *et al*. (2002) developed a quantitative understanding of the propagation of guided Lamb waves in multi-layered, adhesive bonded components by using analytical and computational models. Tang (1999) studied ultrasonic techniques to nondestructively evaluate adhesive bond degradation by introduction of an external factor which pulls the adhesive bond in the nonlinear range, simultaneously with the application of an ultrasonic technique. Wang *et al*. (2009) studied wave propagation along the steel rebar in the concrete where scalar damage parameters characterizing changes in the interface are incorporated into the formulation of the spectral finite element for damage detection of reinforced concrete structures. Su *et al*. (2006) provided a comprehensive review on the state of the art of Lamb wave-based damaged identification approaches for composite structures.

The characteristics of guided waves propagation in adhesively bonded composite to composite structures by using semi-analytical finite element method and Hamilton's principle. A 16 layer adhesive bonded model is used for both plate and pipe structures in the numerical calculation. The phase velocity dispersions and wave structures are presented.

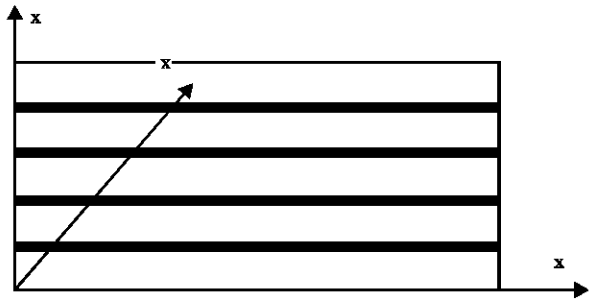

Fig. 1: Composite-to-composite adhesively bonded plate model

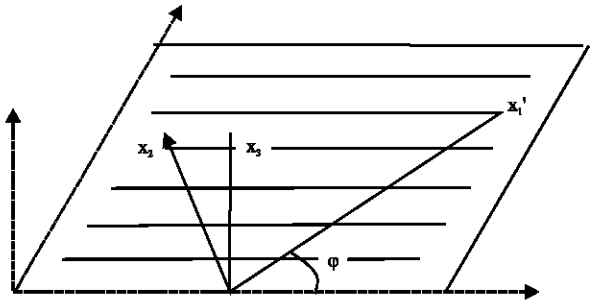

Fig.2: Relationship between principle direction and the g Lo bal direction in rectangular coordinate system

ADHESIVELY BONDED COMPOSITE PLATE

Problem statement: The wave propagates along direction x_1 with wave number k and frequency ω. The cross section lies in the x_2-x_3 plane, as shown in Fig. 1. The displacement, stress and strain field components at each point of the waveguide are expressed by:

$$u = [u_1 \quad u_2 \quad u_3]^T \tag{1}$$

$$s = [\sigma_{11} \quad \sigma_{22} \quad \sigma_{33} \quad \sigma_{23} \quad \sigma_{13} \quad \sigma_{12}]^T \tag{2}$$

$$e = [\varepsilon_{11} \quad \varepsilon_{22} \quad \varepsilon_{33} \quad \varepsilon_{23} \quad \varepsilon_{13} \quad \varepsilon_{12}]^T \tag{3}$$

The constitutive relations at a point are given by:

$$s = Ce \tag{4}$$

where, C is stiffness matrix.

Guided wave equations of motion are formulated by using Hamilton's principle. And the variation of the Hamiltonian of the wave guide, which vanish at all material points, is:

$$\delta H = \int_{t_1}^{t_2} \delta(\Phi - K)dt \tag{5}$$

where, Φ is the strain energy and K is the kinetic energy. The strain energy is given by:

$$\Phi = \frac{1}{2}\int_V e^T C e dV \tag{6}$$

The kinetic energy is given by:

$$K = \frac{1}{2}\int_V \ddot{u}^T \rho \ddot{u} dV \tag{7}$$

where, ρ is the mass density.

By substituting Eq. 6 and 7 into Eq. 5, the Hamilton formulation can be rewritten as follow:

$$\int_{t_1}^{t_2}\left[\int_V \delta(e^T)CedV + \int_V \delta(u^T)\rho\ddot{u}dV\right]dt = 0 \tag{8}$$

Material property: In order to study guided wave propagation, the elastic constants of all the layers must be expressed in the global coordinate system (x_1, x_2, x_3). For a composite material, this can be achieved through the rotation of the stiffness matrix of each lamina:

$$C_\varphi = R_1 C R_2^{-1} \tag{9}$$

where, C_φ is the complex stiffness matrix in the global direction of the laminate, C is the complex stiffness matrix in the individual lamina's principle directions, R_1 and R_2 are the rotation matrices from the principle material directions to the global laminate directions:

$$R_1 = \begin{bmatrix} c^2 & s^2 & 0 & 0 & 0 & 2cs \\ s^2 & c^2 & 0 & 0 & 0 & -2cs \\ 0 & 0 & 1 & 0 & 0 & 0 \\ 0 & 0 & 0 & c & -s & 0 \\ 0 & 0 & 0 & s & c & 0 \\ -cs & cs & 0 & 0 & 0 & c^2 - s^2 \end{bmatrix} \quad R_2 = \begin{bmatrix} c^2 & s^2 & 0 & 0 & 0 & cs \\ s^2 & c^2 & 0 & 0 & 0 & -cs \\ 0 & 0 & 1 & 0 & 0 & 0 \\ 0 & 0 & 0 & c & -s & 0 \\ 0 & 0 & 0 & s & c & 0 \\ -2cs & 2cs & 0 & 0 & 0 & c^2 - s^2 \end{bmatrix} \tag{10}$$

where, c = cosφ and s = sinφ. Here, φ is the angle of rotation from lamina's principle direction to the global direction and the value of φ is positive when the rotation is counterclockwise, as shown in Fig. 2.

Safe method: The plate section is discretized in the thickness direction x_3 as showed in Fig. 2, where $x_{3,1}, x_{3,2}, x_{3,3}$ are coordinates of nodes 1,2 and 3 along x_3 direction, by a set of one-dimensional finite elements with

quadratic shape functions and three nodes, with three degrees of freedom per node. The displacement vector can be approximated over the element domain as:

$$u^{(e)}(x_1, x_2, x_3, t) = \begin{bmatrix} \sum_{j=1}^{3} N_j(x_3) U_{x_1 j} \\ \sum_{j=1}^{3} N_j(x_3) U_{x_2 j} \\ \sum_{j=1}^{3} N_j(x_3) U_{x_3 j} \end{bmatrix}^{(e)} e^{i(kx_1 - \omega t)} = N(x_3) q^{(e)} e^{i(kx_1 - \omega t)} \quad (11)$$

where, $N_j(x_3)$ is the shape functions:

$$N(x_3) = \begin{bmatrix} N_1 & 0 & 0 & N_2 & 0 & 0 & N_3 & 0 & 0 \\ 0 & N_1 & 0 & 0 & N_2 & 0 & 0 & N_3 & 0 \\ 0 & 0 & N_1 & 0 & 0 & N_2 & 0 & 0 & N_3 \end{bmatrix} \quad (12)$$

$$x_3 = \begin{bmatrix} N_1 & N_2 & N_3 \end{bmatrix} \begin{bmatrix} x_{3,1} \\ x_{3,2} \\ x_{3,3} \end{bmatrix} \quad (13)$$

$$\begin{cases} N_1 = \frac{1}{2}(\xi^2 - \xi) \\ N_2 = (1 - \xi^2) \\ N_3 = \frac{1}{2}(\xi^2 + \xi) \end{cases} \quad (14)$$

$U_{x_1 j}, U_{x_2 j}, U_{x_3 j}$ are the unknown nodal displacements in the x_1, x_2, x_3 directions:

$$q^{(e)} = \begin{bmatrix} U_{x_1 1} & U_{x_2 1} & U_{x_3 1} & U_{x_1 2} & U_{x_2 2} & U_{x_3 2} & U_{x_1 3} & U_{x_2 3} & U_{x_3 3} \end{bmatrix}^T \quad (15)$$

The strain vector in the element can be represented as a function of the nodal displacements:

$$e^{(e)} = \left[L_{x_1} \frac{\partial}{\partial x_1} + L_{x_2} \frac{\partial}{\partial x_2} + L_{x_3} \frac{\partial}{\partial x_3} \right] N(x_3) q^{(e)} e^{i(kx_1 - \omega t)} = (B_1 + ikB_2) q^{(e)} e^{i(kx_1 - \omega t)} \quad (16)$$

Where:

$$L_{x_1} = \begin{bmatrix} 1 & 0 & 0 \\ 0 & 0 & 0 \\ 0 & 0 & 0 \\ 0 & 0 & 0 \\ 0 & 0 & 1 \\ 0 & 1 & 0 \end{bmatrix} \quad L_{x_2} = \begin{bmatrix} 0 & 0 & 0 \\ 0 & 1 & 0 \\ 0 & 0 & 0 \\ 0 & 0 & 1 \\ 0 & 0 & 0 \\ 1 & 0 & 0 \end{bmatrix} \quad L_{x_3} = \begin{bmatrix} 0 & 0 & 0 \\ 0 & 0 & 0 \\ 0 & 0 & 1 \\ 0 & 1 & 0 \\ 1 & 0 & 0 \\ 0 & 0 & 0 \end{bmatrix}$$

$$B_1 = L_{x_3} N_{,x_3}, B_2 = L_{x_1} N \quad (17)$$

and:

$$N_{,x_3} = N_{,\xi} \frac{d\xi}{dx_3}$$

By considering the total elements in the thickness, Hamilton formulation becomes to:

$$\int_{t_1}^{t_2} \left\{ \bigcup_{e=1}^{m} \left[\int_V \delta(e^{(e)T} C_\varphi^{(e)} e^{(e)} dV + \int_V \delta(u^{(e)T}) \rho^{(e)} \ddot{u}^{(e)} dV \right] \right\} dt = 0 \quad (18)$$

where, m is the total number of elements in the thickness direction and each elements represented a layer in the composite laminates in the study, $C_\varphi^{(e)}$ and $\rho^{(e)}$ are the element's stiffness matrix and mass density, respectively.

By substituting Eq. 16 into 6 and some algebraic manipulation, yields:

$$\int_V \delta(e^{(*)T}) C_\varphi^{(*)} e^{(*)} dV = \delta q^{(*)T} \int_{x_3} \left[B_1^T C_\varphi^{(*)} B_1 - ikB_2^T C_\varphi^{(*)} B_1 + ikB_1^T C_\varphi^{(*)} B_2 + k^2 B_2^T C_\varphi^{(*)} B_2 \right] dx_3 q^{(*)} \quad (19)$$

The element kinetic energy can be written as:

$$\int_V \delta(u^{(e)T}) \rho^{(e)} \ddot{u}^{(e)} dV = -\omega^2 \delta q^{(e)T} \int_{x_3} N^T \rho^{(e)} N dx_3 q^{(e)} \quad (20)$$

Then, substituting Eq. 19-20 into 18 yields:

$$\int_{t_1}^{t_2} \left\{ \bigcup_{e=1}^{n} \delta q^{(e)} \left[k_1^{(e)} + ikk_2^{(e)} + k^2 k_3^{(e)} - \omega^2 m^{(e)} \right] q^{(e)} \right\} dt = 0 \quad (21)$$

Where:

$$\begin{aligned} k_1^{(e)} &= \int_{x_3} \left[B_1^T C_\varphi^{(e)} B_1 \right] dx_3 \\ k_2^{(e)} &= \int_{x_3} \left[B_1^T C_\varphi^{(e)} B_2 - B_2^T C_\varphi^{(e)} B_1 \right] dx_3 \\ k_3^{(e)} &= \int_{x_3} \left[B_2^T C_\varphi^{(e)} B_2 \right] dx_3 \\ m^{(e)} &= \int_{x_3} \left[N^T \rho^{(e)} N \right] dx_3 \end{aligned} \quad (22)$$

Applying standard finite element assembling procedures to Eq. 21:

$$\int_{t_1}^{t_2} \left\{ \delta U^T \left[K_1 + ikK_2 + k^2 K_3 - \omega^2 M \right] U \right\} dt = 0 \quad (23)$$

where, U is the global vector of unknown nodal displacements:

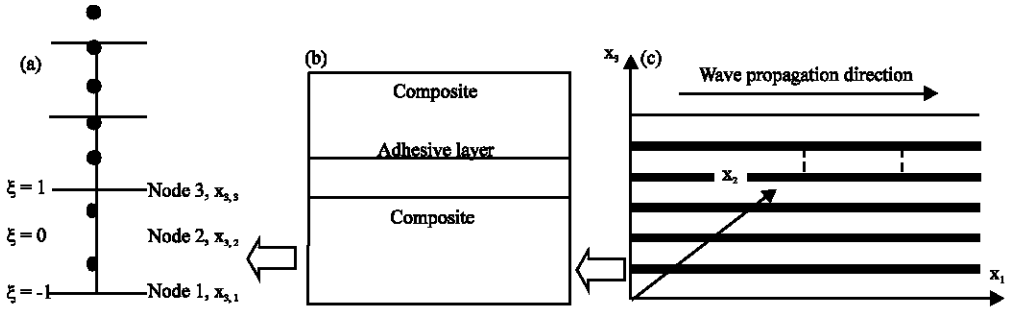

Fig. 3(a-c): SAFE model in adhesively bonded composite-to-composite plate

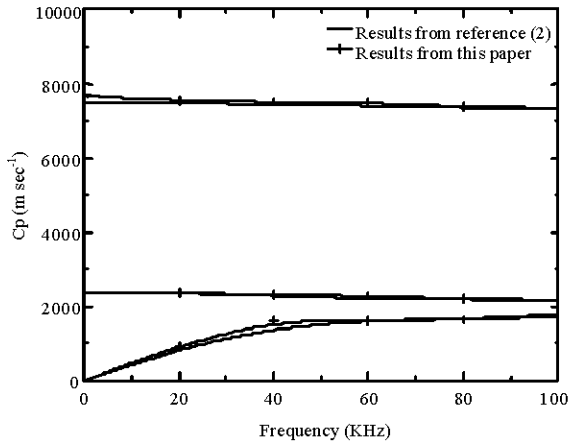

Fig. 4: Comparison of phase velocity curves between Matt (2007) and this paper for composite plate bonded to the spar

$$K_1 = \bigcup_{e=1}^{m} k_1^{(e)}, K_2 = \bigcup_{e=1}^{m} k_2^{(e)}, K_3 = \bigcup_{e=1}^{m} k_3^{(e)}, M = \bigcup_{e=1}^{m} m^{(e)} \quad (24)$$

Due to the arbitrariness of δU, the following wave equation is obtained:

$$\left[K_1 + ikK_2 + k^2K_3 - \omega^2 M\right]U = 0 \quad (25)$$

where, U is the global vector of nodal displacement components. The eigenvalue problem in Eq. 25 relates the wavenumber k to the frequency ω, one of them being given and the other being the eigenvalue to be solved. If k is given, Eq. 25 is a eigenvalue problem with m real eigenvalues ω^2. If instead ω is given, Eq. 25 is a eigenvalue problem with 2 m eigenvalues k.

Numerical results: First, the numerical results are compared with the previous works in Fig. 4. The phase velocity dispersion results obtained from present work for wave propagation analysis in $[0/45/-45/0]_s$ plate bonded to the spar with properly adhesive are compared with the results from Matt (2007). Computations are carried out by taking stiffness coefficients, geometric and physical properties as considering in the reference. The comparison performed in this figure shows that the present results agreed well with those in Matt (2007).

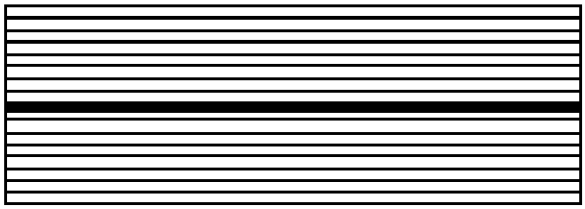

Fig. 5: Sixteen layer adhesively bonded composite plate model and its stacking sequence

Then, a 16 layer adhesively bonded composite model $[(0°/45°/90°/-45°)_s]_2$ is introduced as shown in Fig. 5. The guided wave assumed propagation along the positive x_1 direction which is the fiber direction of the first layer. The material properties of composite and adhesively bonded layer are presented in Matt (2007).

Figure 6 showed the phase velocity dispersion curves about three different adhesive ways: properly bonded, poorly bonded and disbond. The result showed that phase velocity curves are trended to two values and the curves decreased gradually with the bonded situation changing from properly to disbond.

Figure 7-9 presented effects of variation of adhesive layer thickness to phase velocity dispersion curves for three adhesive ways where, h_1 is the thickness of the adhesive layer. The results showed that all the phase velocity curves decreased when the adhesive thickness doubled. Figs.10-12 showed the wave structures of three adhesive bonded composite models in the thickness direction with frequency 50KHz and different phase velocities. The results showed that the amplitudes of phase velocity around 5800 m sec^{-1} are much smaller than around

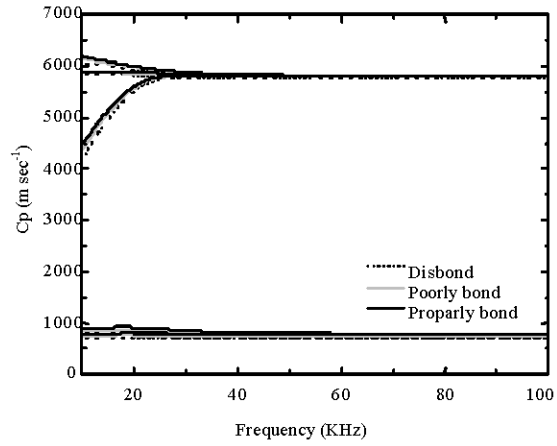

Fig. 6: Phase velocity dispersion curves (properly bonded, poorly bonded and disband)

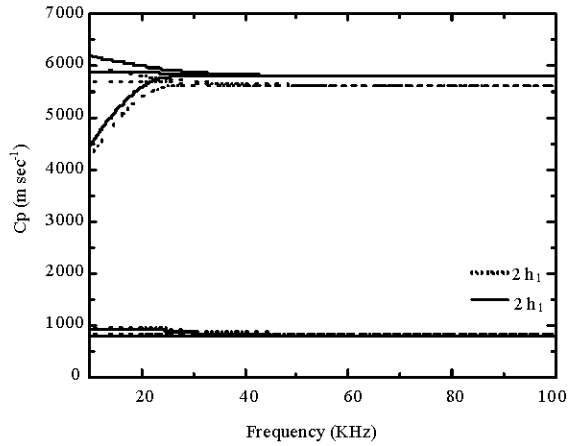

Fig. 7: Phase velocity dispersion curves of properly bonded model with variation of thickness of adhesive layer

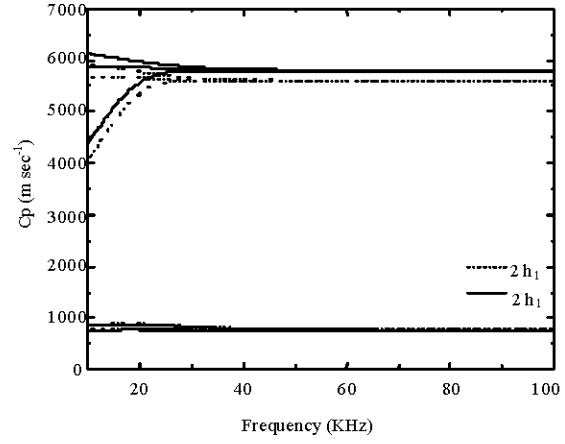

Fig. 8: Phase velocity dispersion curves of poorly bonded model with variation of thickness of adhesive layer

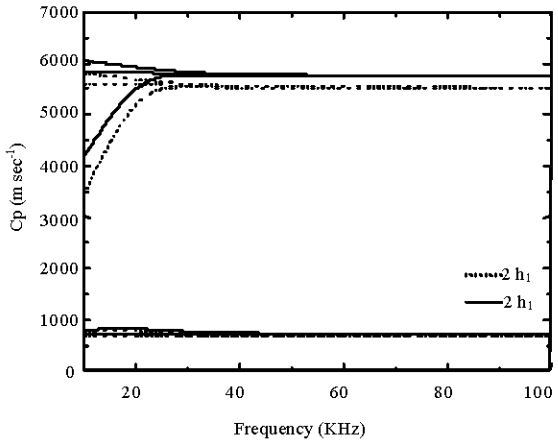

Fig. 9: Phase velocity dispersion curves of disband model with variation of thickness of adhesive layer

800 m sec^{-1}. Fig. 13 showed the comparison of wave structures of different adhesive ways with frequency 580KHz and phase velocity around 800 m sec^{-1} in x_1, x_2, x_3 directions. The amplitudes in the adhesive layer of disbond way are closely zero values.

Adhesively bonded pipe: Consider guided wave propagation along x_3 direction with wave number k and frequency ω. Both outer and inner surfaces of the pipe are assumed to be traction free. The displacement, stress and strain field components at each point of the waveguide are expressed by:

$$u = \left[u_r \quad u_\theta \quad u_3\right]^T \tag{26}$$

$$s = \left[\sigma_{rr} \quad \sigma_{\theta\theta} \quad \sigma_{33} \quad \sigma_{\theta 3} \quad \sigma_{r3} \quad \sigma_{r\theta}\right]^T \tag{27}$$

$$e = \left[\varepsilon_{rr} \quad \varepsilon_{\theta\theta} \quad \varepsilon_{33} \quad \varepsilon_{\theta 3} \quad \varepsilon_{r3} \quad \varepsilon_{r\theta}\right]^T \tag{28}$$

The constitutive relations at a point are given by:

$$\sigma = C\varepsilon \tag{29}$$

Material property: As described in plate situation, the elastic constants of all the layers in composite-to-composite pipe must be expressed in the global coordinate system (r, θ, x_3). For a composite material, this can be achieved through the rotation of the stiffness matrix of each lamina. As showed in Fig. 15a, b, the coordinate axes are labeled as x_1, x_2, x_1', x_2' to correspond with the rectangular coordinate system. To describe the

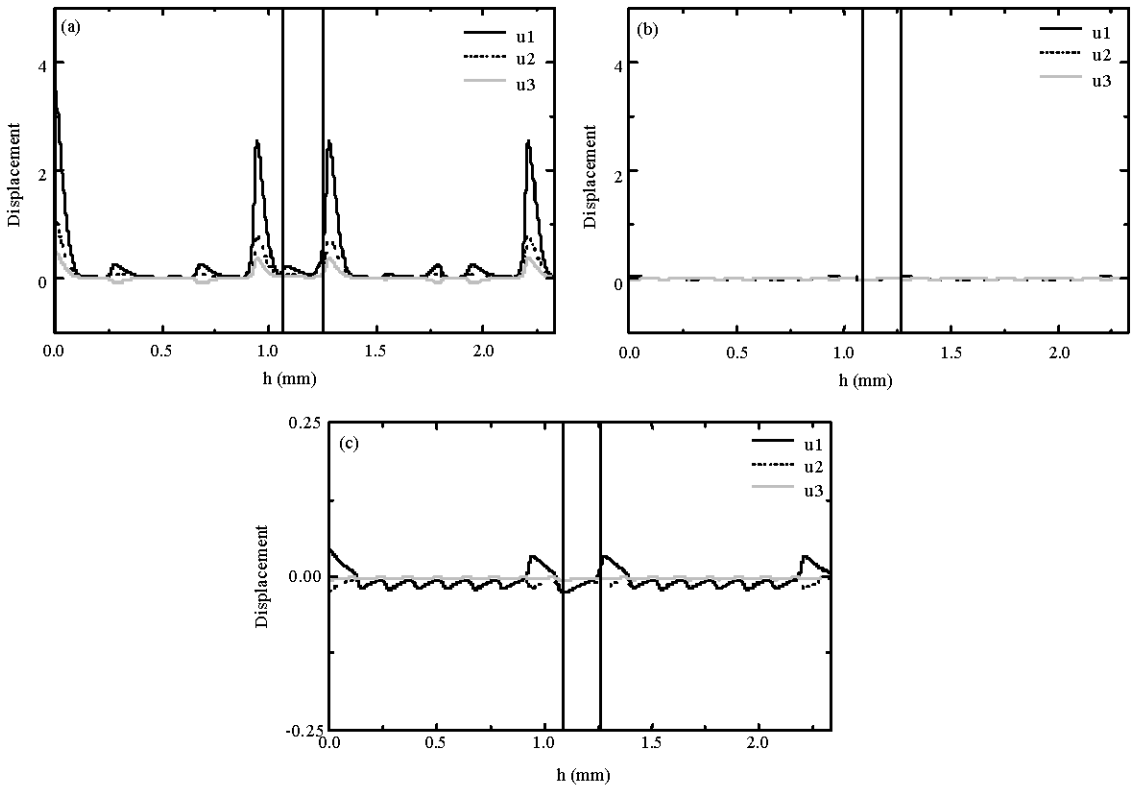

Fig. 10(a-c): Wave structures of properly bonded composite in the thickness direction

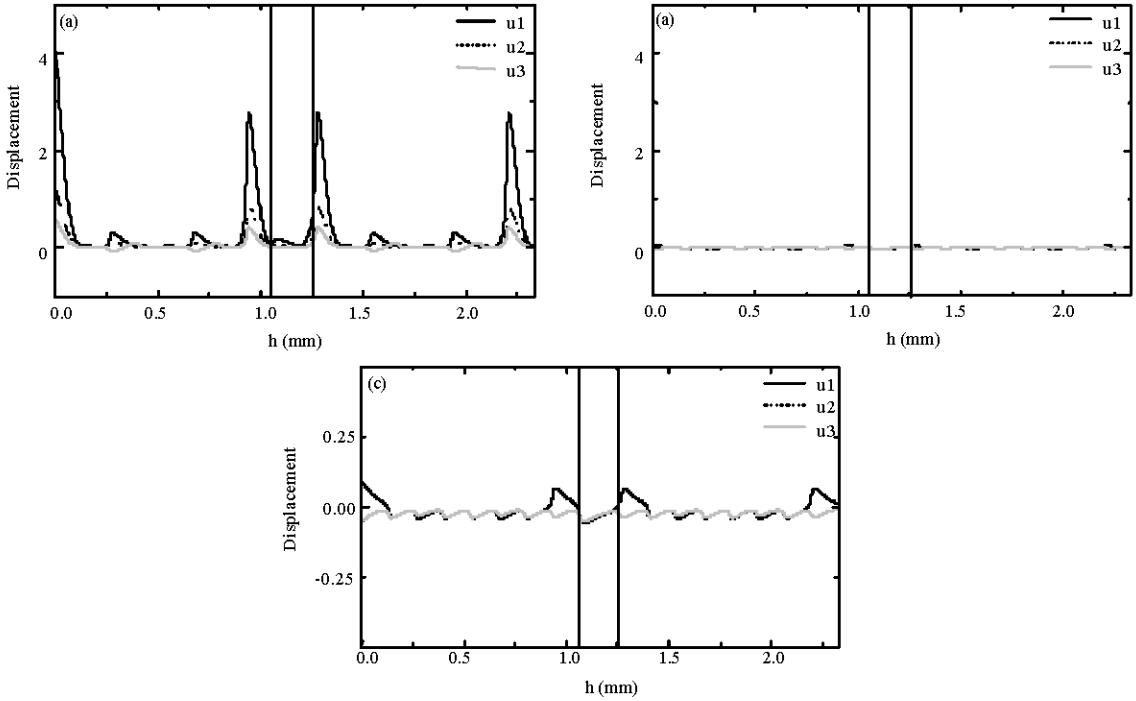

Fig. 11(a-c): Wave structures of poorly bonded composite in the thickness direction

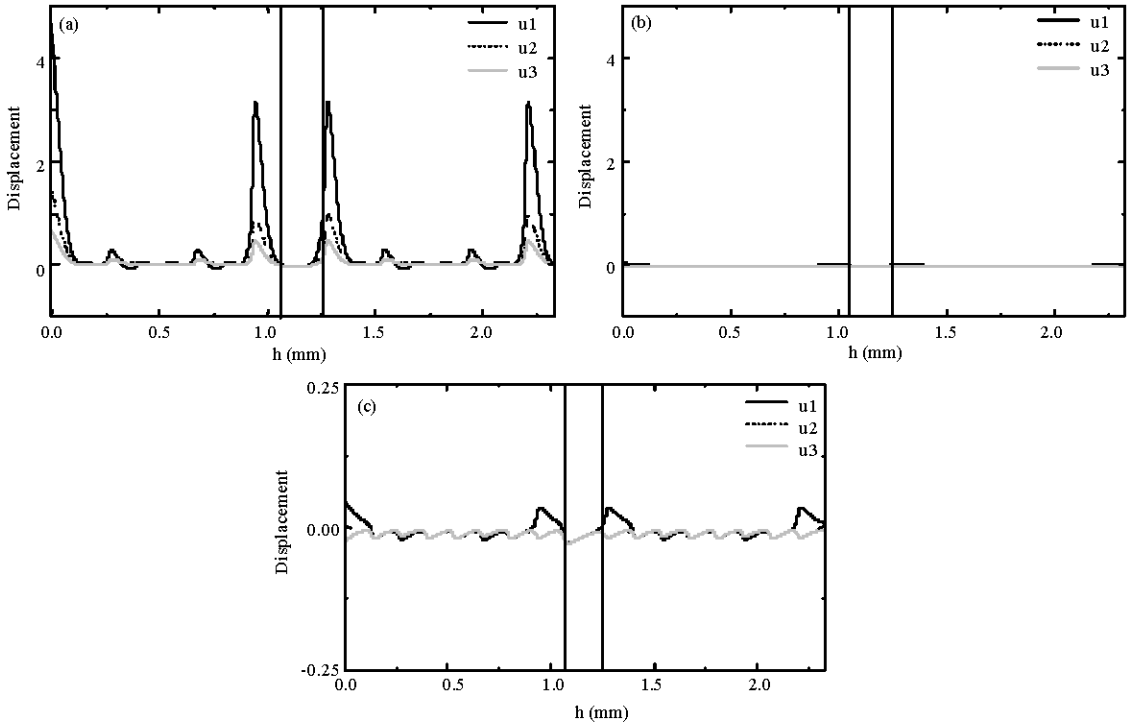

Fig.12: Wave structures of disbond composite in the thickness direction

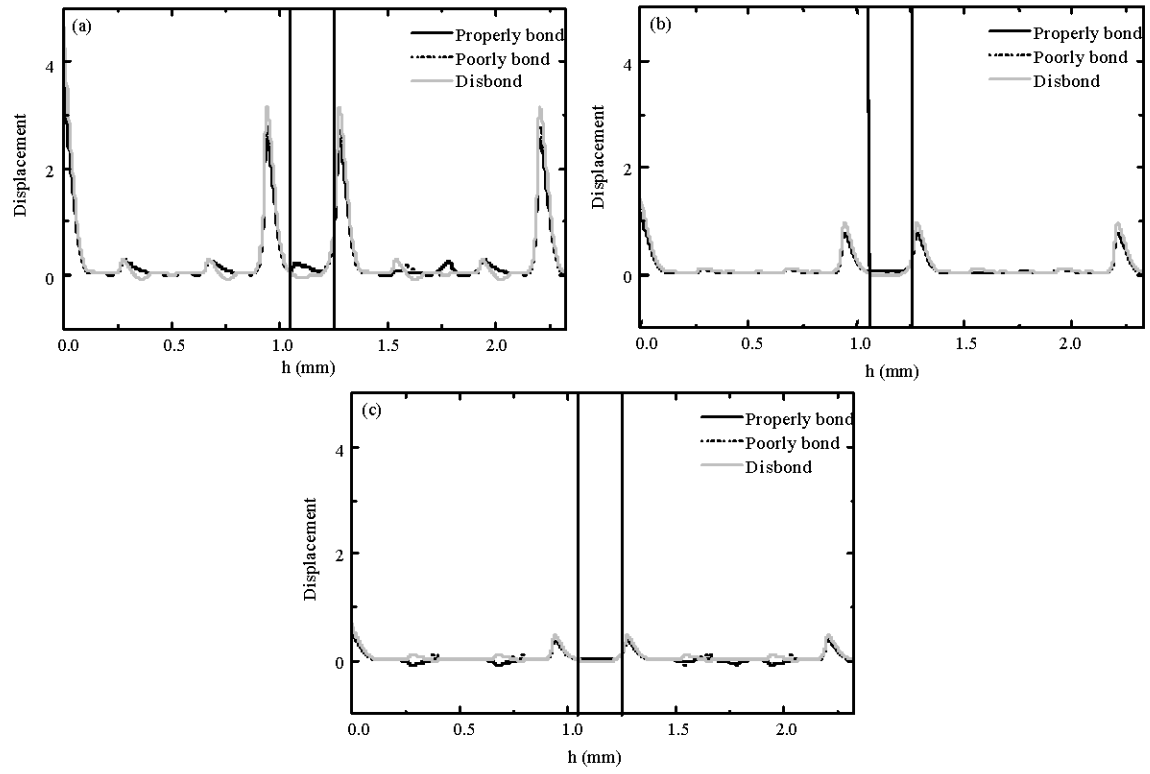

Fig.13: Wave structures of composite in the thickness direction (properly bonded, poorly bonded and disbond)

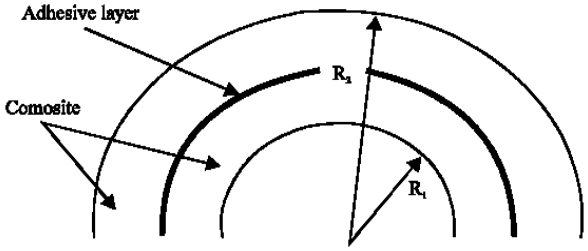

Fig. 14: Composite-to-composite adhesive bonded pipe model

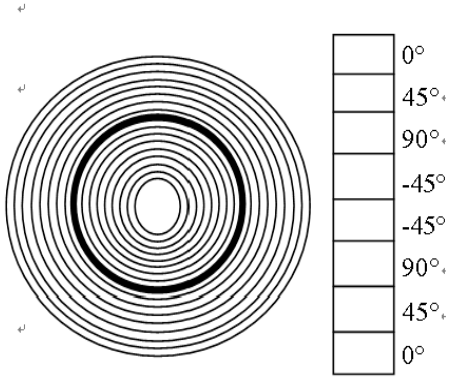

Fig. 15: The 16 layer adhesively bonded composite pipe

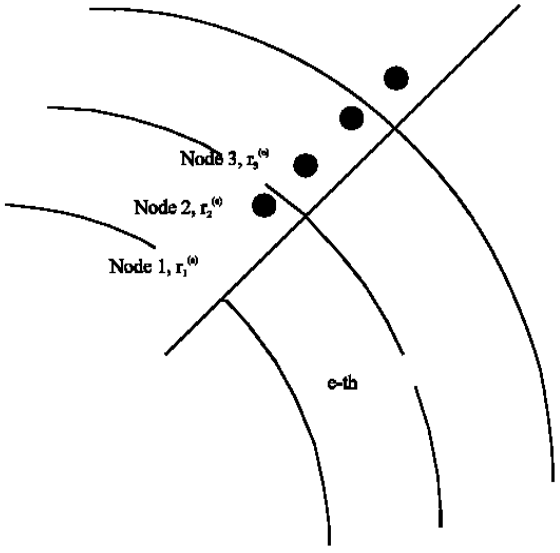

Fig. 16: SAFE model in adhesively bonded composite-to-composite pipe

material property in global cylindrical system (r, θ, x_3), the rotation matrices in Eq. 10 requires rotation, the new rotation matrices are obtained as follow:

$$R_1=\begin{bmatrix}1&0&0&0&0&0\\0&c^2&s^2&2cs&0&0\\0&s^2&c^2&-2cs&0&0\\0&-cs&cs&c^2-s^2&0&0\\0&0&0&0&c&-s\\0&0&0&0&s&c\end{bmatrix}\quad R_2=\begin{bmatrix}1&0&0&0&0&0\\0&c^2&s^2&cs&0&0\\0&s^2&c^2&-cs&0&0\\0&-2cs&2cs&c^2-s^2&0&0\\0&0&0&0&c&-s\\0&0&0&0&s&c\end{bmatrix} \tag{30}$$

where, c = cosφ and s = sinφ. Here, φ is the angle of rotation from lamina's principle direction to the global direction and the value of φ is positive when the rotation is counterclockwise.

Safe method: The pipe is discretized along the radius r throughout thickness of the cross-section and the discretization is reduced to a line of element along the radius of the waveguide as shown in Fig. 16.

The displacement field in the generic e-th finite element can be approximated as:

$$u^{(e)}=N(r)q^{(e)}e^{i(n\theta+kx_3-\omega t)}$$

where, N (r) is the shape function matrix and $q^{(e)}$ is the vector of nodal displacement components in r, θ, x_3 direction:

$$N(r)=\begin{bmatrix}N_1&0&0&N_2&0&0&N_3&0&0\\0&N_1&0&0&N_2&0&0&N_3&0\\0&0&N_1&0&0&N_2&0&0&N_3\end{bmatrix} \tag{31}$$

$$r=\begin{bmatrix}N_1&N_2&N_3\end{bmatrix}\begin{bmatrix}r_1^{(e)}\\r_2^{(e)}\\r_3^{(e)}\end{bmatrix} \tag{32}$$

$$\begin{cases}N_1(r)=1-3r+2r^2\\N_2(r)=4r-4r^2\\N_3(r)=-r+2r^2\end{cases} \tag{33}$$

$$q^{(e)}=\begin{bmatrix}U_{r1}&U_{\theta1}&U_{x_31}&U_{r2}&U_{\theta2}&U_{x_32}&U_{r3}&U_{\theta3}&U_{x_33}\end{bmatrix}^T \tag{34}$$

The strain vector in the element can be represented as a function of the nodal displacements:

$$\begin{aligned}e^{(e)}&=\left[ikL_1+inL_2\frac{1}{r}+L_3\frac{\partial}{\partial r}+L_4\frac{1}{r}\right]N(r)q^{(e)}e^{i(n\theta+kx_3-\omega t)}\\&=(ikB_1+inB_2+B_3)q^{(e)}e^{i(n\theta+kx_3-\omega t)}\end{aligned} \tag{35}$$

Where:

$$L_1=\begin{bmatrix}0&0&0\\0&0&0\\0&0&1\\0&1&0\\1&0&0\\0&0&0\end{bmatrix}\ L_2=\begin{bmatrix}0&0&0\\0&1&0\\0&0&0\\0&0&1\\0&0&0\\1&0&0\end{bmatrix}\ L_3=\begin{bmatrix}1&0&0\\0&0&0\\0&0&0\\0&0&0\\0&0&1\\0&1&0\end{bmatrix}\ L_4=\begin{bmatrix}0&0&0\\1&0&0\\0&0&0\\0&0&0\\0&0&0\\0&-1&0\end{bmatrix} \tag{36}$$

$$B_1=L_1N(r),B_2=L_2\frac{N(r)}{r},B_3=L_3\frac{\partial N(r)}{\partial r}+L_4\frac{N(r)}{r}$$

The dispersion equation is formulated by using the Hamilton's principle in Eq. 5. The variation of the Hamiltonian of the waveguide is presented as:

$$\delta H=\int_{t_1}^{t_2}\bigcup_{e=1}^{m}\left[\delta\Phi^{(e)}-\delta T^{(e)}\right]dt \tag{37}$$

where, m is the number of elements along the radius r. $\delta\Phi^{(e)}$ and $\delta T^{(e)}$ are element strain energy and kinetic energy which can be expressed in cylindrical coordinates as:

$$\delta\Phi^{(e)}=\int_{-\infty}^{+\infty}\int_0^{2\pi}\int_{r_1^{(e)}}^{r_2^{(e)}}\delta[e^{(e)}]^TC_\varphi^{(e)}e^{(e)}rdrd\theta dx_3 \tag{38}$$

$$\delta T^{(e)}=\int_{-\infty}^{+\infty}\int_0^{2\pi}\int_{r_1^{(e)}}^{r_2^{(e)}}[\dot{u}^{(e)}]^T\dot{u}^{(e)}\rho^{(e)}rdrd\theta dx_3 \tag{39}$$

By substituting Eq. 35 into 38 and some algebraic manipulation, yields:

$$\delta\Phi^{(e)}=\delta q^{(e)T}[k^2k_1^{(e)}+knk_2^{(e)}+ikk_3^{(e)}+n^2k_4^{(e)}+ink_5^{(e)}+k_6^{(e)}]q^{(e)} \tag{40}$$

Where:

$$\begin{aligned}k_1^{(e)}&=\int_{r_1^{(e)}}^{r_3^{(e)}}r[B_1^TC_\varphi^{(e)}B_1]dr\\k_2^{(e)}&=\int_{r_1^{(e)}}^{r_3^{(e)}}r[B_2^TC_\varphi^{(e)}B_1+B_1^TC_\varphi^{(e)}B_2]dr\\k_3^{(e)}&=\int_{r_1^{(e)}}^{r_3^{(e)}}r[B_3^TC_\varphi^{(e)}B_1-B_1^TC_\varphi^{(e)}B_3]dr\\k_4^{(e)}&=\int_{r_1^{(e)}}^{r_3^{(e)}}r[B_2^TC_\varphi^{(e)}B_2]dr\\k_5^{(e)}&=\int_{r_1^{(e)}}^{r_3^{(e)}}r[B_3^TC_\varphi^{(e)}B_2-B_2^TC_\varphi^{(e)}B_3]dr\\k_6^{(e)}&=\int_{r_1^{(e)}}^{r_3^{(e)}}r[B_3^TC_\varphi^{(e)}B_3]dr\end{aligned} \tag{41}$$

The element kinetic energy can be written as:

$$\delta T^{(e)}=\delta q^{(e)T}[\omega^2m^{(e)}]q^{(e)} \tag{42}$$

Where:

$$m^{(e)}=\int_{r_1^{(e)}}^{r_3^{(e)}}r[N^T\rho^{(e)}N]dr$$

Then, substituting Eq. 40-42 into Eq. 37 yields:

$$\int_{t_1}^{t_2}\left\{\bigcup_{e=1}^{m}\delta q^{(e)}\left[k^2k_1^{(e)}+knk_2^{(e)}+ikk_3^{(e)}+n^2k_4^{(e)}+ink_5^{(e)}+k_6^{(e)}-\omega^2m^{(e)}\right]q^{(e)}\right\}dt=0 \tag{43}$$

Applying standard finite element assembling procedures to Eq. 43:

$$\int_{t_1}^{t_2}\left\{\delta U^T\left[k^2K_1+knK_2+ikK_3+n^2K_4+inK_5+K_6-\omega^2M\right]U\right\}dt=0 \tag{44}$$

where, U is the global vector of unknown nodal displacements:

$$\begin{gathered}K_1=\bigcup_{e=1}^{m}k_1^{(e)},K_2=\bigcup_{e=1}^{m}k_2^{(e)},K_3=\bigcup_{e=1}^{m}k_3^{(e)},K_4=\bigcup_{e=1}^{m}k_4^{(e)},\\K_5=\bigcup_{e=1}^{m}k_5^{(e)},K_6=\bigcup_{e=1}^{m}k_6^{(e)},M=\bigcup_{e=1}^{m}m^{(e)}\end{gathered} \tag{45}$$

Due to the arbitrariness of δU, the following wave equation is obtained:

$$\left[k^2K_1+knK_2+ikK_3+n^2K_4+inK_5+K_6-\omega^2M\right]U=0 \tag{46}$$

where, U is the global vector of nodal displacement components. Eq. 46 has the form of a three parameter algebraic eigensystem, depending on the circular frequency ω and on both longitudinal wave numbers k and circumferential wave numbers n. Here, n is assigned to obtain the n-th order axial symmetric modes and k is adopted as the eigenvalue parameter for a given frequency ω.

NUMERICAL RESULTS

A 16 layer adhesively bonded composite pipe model $[(0^\circ/45^\circ/90^\circ/-45^\circ)_s]_2$ is studied. The inner radius of the composite pipe model is 100 mm. The guided wave assumed propagation along the positive x_3 direction which is the fiber direction of the first layer. The material properties of composite and adhesively bonded layer are presented in Matt (2007).

Figures 17-19 showed the phase velocity dispersion curves about three different adhesive ways: properly bonded, poorly bonded and disbond by giving n = 1, 2, 3.

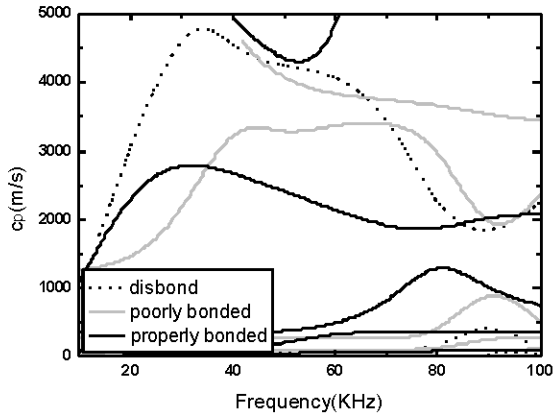

Fig.17: Phase velocity dispersion curves with (properly bonded, poorly bonded and disband)

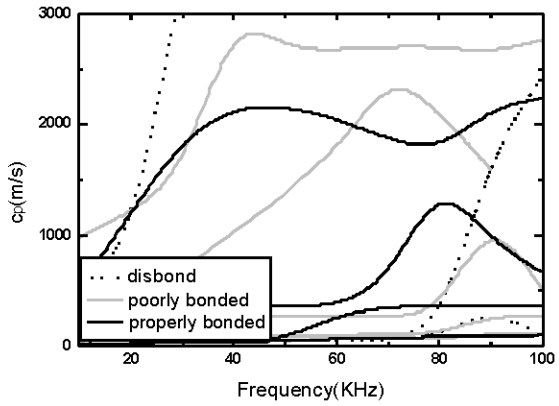

Fig. 18: Phase velocity dispersion curves with (properly bonded, poorly bonded and disband)

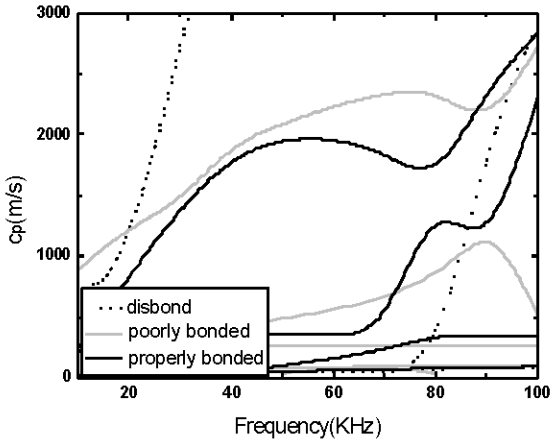

Fig. 19: Phase velocity dispersion curves with (properly bonded, poorly bonded and disband)

The results showed that the differences between three adhesive ways are noticeable and the dispersion of phase velocity could be used as a feasible tool for identification of the state of the adhesive layer in composite-to-composite pipe.

CONCLUSION

The characteristics of guided waves in adhesively bonded composite-to-composite structures are studied in the paper. The semi-analytical finite element method and Hamilton's principle are used to model and solve the problem. Both plate model and pipe model are analyzed through mathematic formulations and numerical calculations, the phase velocity dispersion curves and wave structures are presented. The results showed some useful suggestion for inspection adhesively bonded composite structures by guided waves.

REFERENCES

Allin, J.M, P. Cawley and M.J.S. Lowe, 2003. Adhesive disbond detection of automotive components using first mode ultrasonic resonance. NDT and E Int., 36: 503-514.

Brotherhood, C.J., B.W. Drinkwater and S. Dixon, 2003. The detectability of kissing bonds in adhesive joints using ultrasonic techniques. Ultrasonics, 41: 521-529.

Di Scalea, F.L., P. Rizzo and A. Marzani, 2004. Propagation of ultrasonic guided waves in lap-shear adhesive joints: Case of incident a_0 Lamb wave. J. Acoust. Soc. Am., 115: 146-156.

Duflo, H., B. Morvan and J.L. Izbicki, 2007. Interaction of Lamb waves on bonded composite plates with defects. Compos. Struct., 79: 229-233.

Higgins, A., 2000. Adhesive bonding of aircraft structures. Int. J. Adhesion Adhesives, 20: 367-376.

Lowe, M.J.S., R.E. Challis and C.W. Chan, 2000. The transmission of Lamb waves across adhesively bonded lap joints. J. Acoust. Soc. Am., 107: 1333-1345.

Matt, H., 2007. Structural diagnostics of CFRP composite aircraft components by ultrasonic guided waves and built-in piezoelectric transducers. Ph.D. Thesis, University of California, USA.

Matt, H., I. Bartoli and F.L. di Scalea, 2005. Ultrasonic guided wave monitoring of composite wing skin-to-spar bonded joints in aerospace structures. J. Acoust. Soc. Am., 118: 2240-2252.

Seifried, R., L.J. Jacobs, J.M. Qu, 2002. Propagation of guided waves in adhesive bonded components. NDT. E. Int., 35: 317-328.

Su, Z.Q., L. Ye and Y. Lu, 2006. Guided Lamb waves for identification of damage in composite structures: A review. J. Sound Vibr., 295: 753-780.

Tang, Z.Z., 1999. Ultrasonic nondestructive evaluation of adhesive bond degradation. Ph.D. Thesis, Northwestern University, Chicago, IL., USA.

Wang, Y., X.Q. Zhu, H. Hao and J.P. Ou, 2009. Guided wave propagation and spectral element method for debonding damage assessment in RC structures. J. Sound Vibr., 324: 751-772.